Journal of Materials Chemistry B

PAPER

View Article Online
View Journal

Cite this: DOI: 10.1039/c4tb01310g

Aptamer-mediated nanocomposites of semiconductor quantum dots and graphene oxide as well as their applications in intracellular imaging and targeted drug delivery†

Li Zhang,[ab] Sai Jin Xiao,[ac] Lin Ling Zheng,[a] Yuan Fang Li[a] and Cheng Zhi Huang*[a]

Received 7th August 2014
Accepted 6th October 2014

DOI: 10.1039/c4tb01310g

www.rsc.org/MaterialsB

Fluorescent semiconductor quantum dot–graphene oxide (QD–GO) nanocomposites with unique optical properties can be prepared by a facile decoration of aptamer-labelled CdSe@ZnS QDs on GO nanosheets. The formation of such nanocomposites is based on the π–π stacking between the DNA bases on the QD surfaces and the GO. TEM and AFM were used to study the morphologies and distribution of the QDs on the GO surfaces. Steady-state fluorescence spectra, time-resolved fluorescence experiments and fluorescence imaging were employed to study the optical properties of the prepared aptamer-QD–GO nanocomposites. Furthermore, we investigate the potential applications of the nanocomposites in bio-imaging and cell-targeted drug delivery. The QDs decorated on the surfaces of GO could serve as fluorescent labeling probes for tracking the intracellular transport, while the GO combined with the aptamer conjugated on the outside of the nanocomposites facilitates the targeted drug delivery with enhanced loading capability. It is believed that the present aptamer-QD–GO nanocomposite-based nanomedicine would permit the development of more effective means for diagnosing and treating malignancies compared to the currently used methods.

Published on 06 October 2014. Downloaded on 31/10/2014 00:31:00.

Introduction

Graphene, as an atomic-layer-thick 2D system, has triggered considerable research interest owing to its unique optical,[1] electronic,[2] magnetic,[3] and mechanical properties.[4] These fascinating properties of graphene make it a promising candidate for electronic devices,[5] sensitive chemical sensors,[6] photothermal agents,[7] composite materials,[8] and especially as a transporter for intercellular drug delivery owing to its biocompatibility and nontoxicity at the cellular level.[9–12] The difficulties one has to be confronted with when applying graphene and its derivatives in sensing *in vivo* and drug delivery are how to trace the dynamic route of graphene without visible emission in cells and further to observe whether it is cleared off quickly by cells or stays for a period of time after completion of its mission. Clarification of these issues is of great significance. For this purpose, various optical probes such as light scattering nanoparticles and fluorescent dyes have been successfully decorated on graphene to directly trace its dynamic route and clarify its behaviors in organisms. For example, our group has recently decorated metal nanoparticles on carbon nanotubes/graphene sheets and demonstrated the potential application of these novel nanocomposites in dark field microscopic imaging (iDFM) in a light scattering fashion.[13,14] The limitation of iDFM was that the large size of metal nanoparticles might influence the internalization process, and the dynamic tracking as well as the trajectory analysis of the nanocomposites cannot be accomplished due to the limitation of dark field light scattering techniques. While the approaches related to immobilization of fluorescent organic species on GO suffer from less quantum yield,[15] photobleaching, elaborate design and complex functionalization procedures.[16]

Compared with organic fluorophores, semiconductor quantum dots (QDs) as a new class of fluorescent probes involve more unique optical characteristics (high quantum yield, good photostability and large Stokes shift),[17] which have been widely applied in the area of biosensing,[18] immunoassays,[19,20] and especially biological imaging.[21] Therefore, the construction of nanocomposites composed of QDs and GO might not only provide visualization by conventional microscopy for cellular imaging due to the excellent fluorescence properties of QDs, but also help in solving the transport problems for pharmacologically relevant compounds that need to be internalized.

[a]Key Laboratory of Luminescent and Real-Time Analytical Chemistry, Ministry of Education, College of Pharmaceutical Sciences, College of Chemistry and Chemical Engineering, Southwest University, Chongqing, 400715, China. E-mail: chengzhi@swu.edu.cn; Tel: +86-23-68254659

[b]Department of Chemistry, Nanchang University, Nanchang, 330031, China

[c]Jiangxi Key Laboratory of Mass Spectrometry and Instrumentation, East China Institute of Technology, Nanchang, 330013, China

† Electronic supplementary information (ESI) available: Fig. S1–S4. See DOI: 10.1039/c4tb01310g

Published on 06 October 2014. Downloaded on 31/10/2014 00:31:00.

QD–GO nanocomposites could be prepared by *in situ* growth,[22,23] non-covalent adsorption and chemical modification.[24–27] However, a key disadvantage of *in situ* growth methods is the difficulty in defining and controlling the spatial coverage and distribution of QDs. While covalently modifying the GO surface by using functional groups for creating QD–GO hybrids involves a relatively complex and time-consuming protocol, and the covalent bonds may disrupt the initial structure of GO and thus change its optical and electronic properties. Conversely, the non-covalent methods could not only enhance its solubility and processability, but also maintain the integrity and hence the corresponding optoelectronic properties of GO. Additionally, the morphology and thus the optical properties of individual QDs can be easily tailored by sophisticated synthesis methods prior to combination with GO, thereby mitigating the influence of GO themselves on the nucleation and growth processes of QDs. Another issue should be noticed is that most of the previously fabricated QD–GO or QD–CNT nanocomposites possess no fluorescence activity due to the quenching effect by GO and CNTs, which would limit their applications as optical probes for further chemical sensing and biological imaging. It is conceivable that by regulating the space between QDs and carbon nanoparticles through macromolecule bridging (such as surfactants, protein, and DNA) or a silica shell might help to retain the fluorescence of the QDs.[7,28–30]

Along this line in this contribution, we report the preparation (Fig. 1) of a highly versatile multicomponent nanosystem by decorating aptamer-modified QDs on the GO surfaces, where the aptamer could not only serve as a linkage to bridge QDs and GO through the π–π stacking but also act as a recognition unit to target the cellular prion protein (PrP^C) overexpressed in the human bone marrow neuroblastoma (SK-N-SH cells).[31] The maintained fluorescent labeling behavior of decorated QDs facilitates the application of the nanosystem in cell imaging and the extremely high aspect ratio of GO makes the nanocomposite a good scaffold for intracellular drug delivery due to its improved drug loading capacity. This nanocomposite has overcome several of the obstacles in previous research: the fluorescence quenching is greatly reduced by maintaining a precisely controlled DNA spacer between the QDs and the GO. Remarkably, active targeting and enhanced cell internalization through the conjugation of the QD–GO with targeting/internalization ligands (aptamer) have also been achieved, where the aptamer could be rationally designed for different types of cells. The integration of these functionalities makes this nanocomposite a potentially viable new tool for disease diagnosis, imaging and treatment through drug/molecule delivery.

Results and discussion

Firstly, GO sheets were synthesized by a modified Hummers method.[32,33] The QDs were functionalized with the prion protein aptamer *via* covalent bonding, and the detailed process could be found in the experimental section. The prepared aptamer-QD conjugates were characterized by the FTIR spectrum. As shown in Fig. S1 in the ESI,† the bands at 1642 and 1238 cm^{-1} represent the secondary amide C=O and C–N stretching vibrations,[34] while the weak band at 1469 cm^{-1} reflects the ring vibration of the DNA bases, and the peaks at 1200 and 1112 cm^{-1} correspond to the asymmetric and symmetric PO_2^- groups of the DNA backbone.[35] These data reveal that the aptamer DNA has been successfully bonded to the QD surface. The prepared GO powder was mixed with aptamer-QD solution, sonicated for 30 min, and then allowed to stand overnight so that undispersed GO sedimented. The resulting clear supernatant was carefully collected by centrifugation to remove QDs not bound to the GO sheet, and the redispersed solution will henceforth be called aptamer-QD–GO. It was supposed that the DNA modified QDs can successfully self-assemble on the GO sheet *via* π–π stacking due to the conjugated aromatic ring in the bases.[36,37]

The morphologies and distribution of the QDs on the GO surface were characterized by transmission electron microscopy (TEM) images and atomic force microscopy (AFM) images. Fig. 2a shows the TEM image of GO sheets with corrugated flakelike shapes. Mono-layer sheets could be observed in most of the regions, whereas restacked parts and wrinkles could also

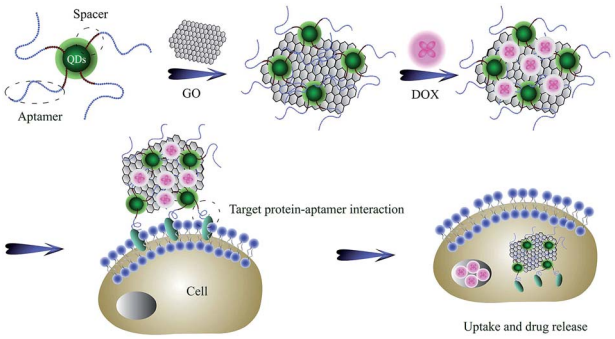

Fig. 1 Schematic presentation of the bio-imaging and cell-targeted drug delivery by using the aptamer-QD–GO nanocomposites.

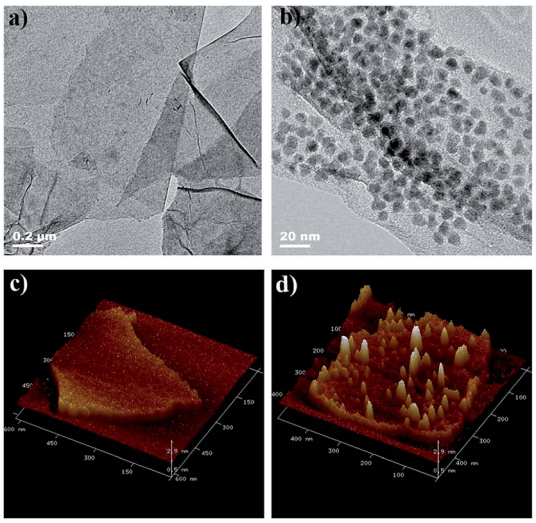

Fig. 2 TEM images of GO (a) and aptamer-QD–GO nanocomposites (b). AFM images of GO (c) and aptamer-QD–GO nanocomposites (d).

This journal is © The Royal Society of Chemistry 2014

Published on 06 October 2014. Downloaded on 31/10/2014 00:31:00.

be seen, which could be attributed to electronic repulsion between the soft and flexible layers. Fig. 2b shows that the individual QDs are well separated from each other and well spread out on the GO sheets. There is neither apparent aggregation of QDs on the GO nanosheets (Fig. S2, ESI†) nor large areas of the GO sheets without QD decoration. The good distribution of QDs on GO nanosheets guarantees unique optical properties of the aptamer-QD–GO hybrid and further efficient molecular adsorption for drug delivery. It was found that these aptamer-QD–GO hybrids were highly stable, without any precipitation and showed only a minimal fluorescence loss after 24 h of ambient storage in phosphate buffered saline (PBS) (results are not shown). Fig. 2c shows that the as-prepared GO prior to the introduction of QDs possessed well-dispersed individual nanosheets with an average thickness of 0.8 nm, indicating the monolayer structure of the obtained GO. Fig. 2d shows the AFM topography of the aptamer-QD–GO hybrid, and the height of the decorated QDs was about 2.4 nm, implying a monolayer of QDs on the GO surfaces.

The optical properties of the QDs and aptamer-QD–GO hybrid were measured using UV-vis absorption spectra and steady-state fluorescence (FL) spectra. Fig. 3a shows the UV-vis absorption spectra of pure GO dispersion, pure colloidal QDs, aptamer-modified QDs, as well as aptamer-QD–GO nanocomposite dispersion. There are two absorption features for GO: a peak at 233 nm due to the $\pi \rightarrow \pi^*$ transition of C=C, and a shoulder at about 300 nm corresponding to the $n \rightarrow \pi^*$ transition of the C=O bond.[25,38] The absorption at 255 nm due to DNA is clearly observed for aptamer-modified QDs, proving successful conjugation of aptamer on the QD surfaces. Moreover, the QDs as well as the aptamer-modified QDs exhibited a well-pronounced absorption peak at about 579 nm, indicating the consequence of quantum confinement of QDs. Furthermore, this obvious spectral feature was also noted in aptamer-QD–GO nanocomposites. Previous investigations reported that no QD absorption band could be observed after QDs were attached to GO because the broad background absorption of GO could strongly screen the absorption of the QDs.[25,39] The large polydispersity in size and shape of the crystallites on the GO surface and the relatively small amount of QDs successfully bound to the GO were also considered as possible explanations for the lack of any absorption band in the composites,[40] only if QDs with uniform morphology were densely coated onto the GO could the absorption band be seen. However, the absorption band of QDs in our experiment could still be observed, which suggests a dense coating of QDs on the GO sheets. Moreover, no obvious change of the absorption band of the QDs was observed, which indicates that almost no QD agglomerate was formed on the GO sheets, consistent with TEM and AFM observations.

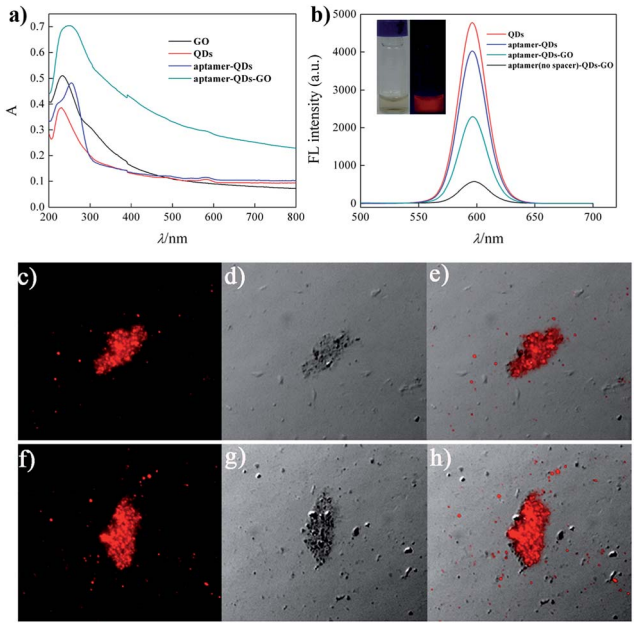

Fig. 3 (a) UV-vis absorption spectra of GO, free QDs, aptamer-QDs, and aptamer-QD–GO, respectively. (b) Fluorescence spectra of free QDs, aptamer-QDs, aptamer-QD–GO, and aptamer (no spacer)–QD–GO, respectively. The inset in (b) shows the aptamer-QD–GO suspensions under visible light (left) and UV light (right). Fluorescence (c) and (f), differential interference contrast (DIC) (d) and (g), and the overlay of DIC and fluorescence mode (e) and (h) of the aptamer-QD–GO nanocomposite.

It should be noticed that the characteristic emission of QDs and aptamer-QD–GO nanocomposites shows an emission band at 605 nm when excited at 365 nm, whereas the fluorescence quantum yield of the aptamer-QD–GO nanocomposites is about 60% of the monodispersed aptamer-QDs without adding the GO nanosheets (Fig. 3b and S3, ESI†). The partial fluorescence quenching can be ascribed to the electron-acceptor behavior of GO. That is, part of the photoexcited electrons produced upon illumination of QDs can conceivably flow into GO non-radiatively, prior to their recombination with photogenerated holes in QDs.[22,39] A similar phenomenon has been previously observed in QD–CNT and QD–GO nanocomposites, especially when the carbon nanomaterials and QDs are in close spatial contact with one another.[23,25,27,41] It is suspected that the present aptamer-QD–GO nanocomposites maintain the majority of fluorescence due to the additional poly A_{10} spacer (estimated length $\approx$ 3.0 nm) which has been previously proven to involve poor π–π stacking ability with GO that can seperate QDs and GO and thus protect the fluorescence of QDs from being quenched.[42,43] In comparison, the fluorescence of its analogue by directly conjugating the QDs with GO through the aptamer linkage is almost completely quenched under identical conditions (Fig. 3b and S3, ESI†), indicating the important role of spacer in maintaining the fluorescence properties. The optical images in the inset illustrate well-dispersed aptamer-QD–GO nanocomposites in water with no aggregation, and strong light emission from aptamer-QD–GO nanocomposites is observed under UV irradiation (inset of Fig. 3b), where the fluorescence emission color can be rationally tuned by changing the QD size, implying the potential application of the nanocomposites in multiplex color bio-imaging.

The optical properties of aptamer-QD–GO nanocomposites could be further characterized by fluorescence images. As shown in Fig. 3c–h, the bright-field image along with the

Published on 06 October 2014. Downloaded on 31/10/2014 00:31:00.

composite merged image clearly correlated the spectral overlap of QD fluorescence with the spatial localization of the GO. Although detailed information about the fluorescence features of individual QDs was not possible due to the limited diffraction resolution of the optical system (due to the numerical aperture of the objective and condenser lenses), the distribution of QD fluorescence on the GO surface was uniform, an observation fully consistent with our TEM data (Fig. 2).

Further characterization and confirmation of QD-to-GO electron transfer were obtained using FL decay time analyses. Fig. 4a and b compare the emission decay traces of pure colloidal QDs, aptamer modified QDs as well as aptamer-QD–GO nanocomposites. The emission kinetics of QDs can be fitted multiexponentially with time constants of $\tau_1 = 2.79$ ns (5.13%), $\tau_2 = 13.6$ ns (48.6%), and $\tau_3 = 27.5$ ns (46.27%). The fluorescence decay kinetics may be governed by both intrinsic and surface states, and it was supposed that the multiexponential decay in the present situation arises from surface traps. Consistent with FL quenching results, DNA modification would not alter the emission decay kinetics of QDs, while decorating on the GO surface successively decreases the FL lifetime of QDs. On the GO surface the emission kinetics of QDs can be fitted with time constants $\tau_1 = 0.83$ ns (17.78%), $\tau_2 = 5.36$ ns (66.06%), and $\tau_3 = 15.1$ ns (16.17%). It is clearly seen from Fig. 4 that the emission kinetics of QDs on the GO surface decay much faster, which is a clear indication of electron transfer from photoexcited QDs. The faster lifetimes appear as a result of the carrier quenching due to the electron accepting nature of GO.

Since the GO used in our contribution demonstrates weak FL emission centered at 540 nm when excited by 370 nm, it is important to compare the lifetime results from the QD decays with the electron acceptor GO decays. As shown in Fig. 4c and d, the emission kinetics of GO can be fitted biexponentially with time constants of $\tau_1 = 0.4$ ns (93.79%) and $\tau_2 = 2.1$ ns (6.21%) following direct optical excitation. However, with the assembly of QDs, the PL decay became distinctly multiexponential, showing a long-lifetime component (22.0 ns) and a residual fast decay component that paralleled the native GO lifetime. The appearance of the long-lifetime decay component that was commensurate with the fast QD FL decay component (27.5 ns) provides conclusive evidence of efficient electron transfer from QDs to GO, which was in good agreement with that estimated from the QD FL decay.[44]

Since the majority of FL has been maintained despite the partial FL quenching as a result of electron transfer, we then investigated whether aptamer-QD–GO nanocomposites could be used as fluorescently detectable intracellular nanoprobes in SK-N-SH cells through specific aptamer-mediated endocytosis by fluorescence microscopy. It is clearly seen from Fig. 5 that the SK-N-SH cells can be successfully fluorescently labeled and imaged by both the red- and green-colored aptamer-QD–GO nanocomposites (Fig. 5). It is suspected that the aptamer conjugated on the outside of the QD–GO nanocomposites can specifically interact with the prion protein on the cellular membranes and be constitutively internalized into the cytoplasm of SK-N-SH cells through a PrP^C-dependent endocytic pathway, and more experiments are in progress to better establish the subcellular distribution and location of the nanocomposites after the cellular uptake.

Having demonstrated the nanocomposite internalization, we were in a position to evaluate the toxicity of the aptamer-QD–GO nanocomposites. The MTT assay was used to evaluate the cytotoxicity of aptamer-QD–GO in incubated SK-N-SH cells. The results revealed negligible differences in cell viability over an incubation period of 12 to 48 h with different concentrations of nanocomposites (Fig. S4, ESI†). We then explored the application of aptamer-QD–GO nanocomposites as sheet-like vehicles

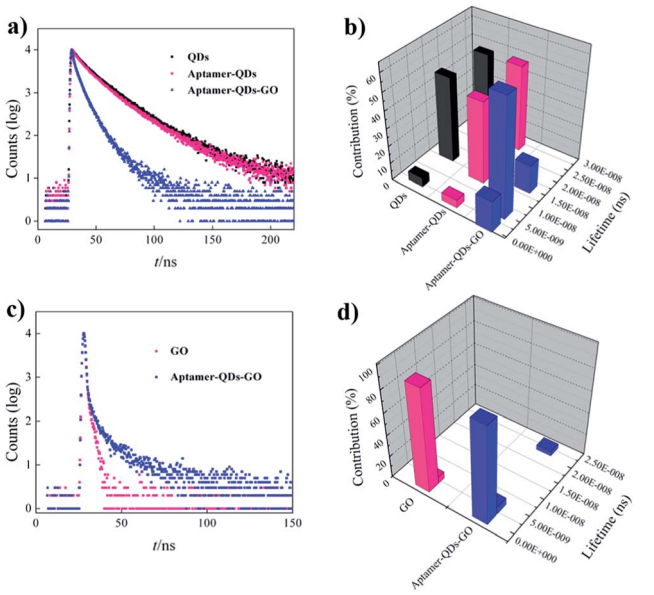

Fig. 4 (a) FL decay of QDs, aptamer-QDs and aptamer-QD–GO as a function of time. (b) PL lifetimes of QDs, aptamer-QDs and aptamer-QD–GO. (c) FL decay of GO and aptamer-QD–GO as a function of time. (d) PL lifetimes of GO and aptamer-QD–GO.

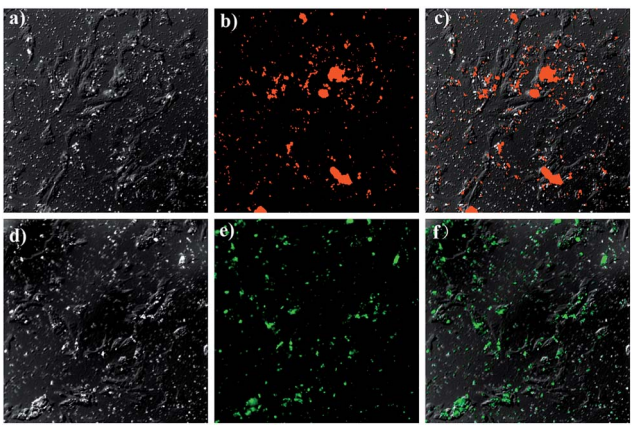

Fig. 5 Delivery of aptamer-QD–GO nanocomposites into the living SK-N-SH cells. Differential interference contrast (DIC) (a) and (d), fluorescence (b) and (e), and the overlay of DIC and fluorescence mode (c) and (f). The images (a)–(c) show the delivery of red-colored aptamer-QD–GO nanocomposites while images (d)–(f) show the delivery of green-colored aptamer-QD–GO nanocomposites.

This journal is © The Royal Society of Chemistry 2014

Published on 06 October 2014. Downloaded on 31/10/2014 00:31:00.

to transport an aromatic drug doxorubicin (DOX), a widely used chemotherapy drug for treating various cancers, into cancer cells. The loading of DOX was performed by simple mixing of the aptamer-QD–GO nanocomposite dispersion with DOX at pH 7.4 overnight, followed by repeated centrifugation to remove free, unbound DOX in solution. The formation of aptamer-QD–GO–DOX was visible from the reddish color due to adsorbed DOX and its characteristic UV-vis absorbance peak at 504 nm, which is red-shifted by 14 nm compared with the DOX in solution (Fig. 6a). The loading of DOX onto GO can be attributed to π–π stacking, hydrophobic as well as hydrogen-bonding interactions,[11,45] similar to that with carbon nanotubes, resulting in fluorescence quenching due to the close proximity of DOX to the GO nanosheets (Fig. 6a). The loading capacity of DOX on the QD–GO hybrid was determined by UV-vis absorption spectra, which was calculated by the difference of DOX concentrations between the original DOX solution and the supernatant solution after loading. The loading amount of DOX on the QD–GO hybrid was investigated in different initial DOX concentrations with respect to the same concentration of QD–GO (0.31 mg mL^{-1}), and the loading of DOX on neat GO is used as a comparison. It was found that the loading amount of DOX on the QD–GO hybrid increased with initial DOX concentrations (Fig. 6b). The saturated loading amount of DOX on the QD–GO hybrid is 1.8 mg mg^{-1} while the amount of DOX loaded on GO can reach 2.78 mg mg^{-1} at a DOX concentration of 1.125 mg mL^{-1}, and the reason could be explained as follows, since the QDs have been assembled onto the GO surfaces *via* π–π stacking between GO and single-stranded aptamer, it is expected that the aptamer-QD conjugates would occupy some surface areas on GO and thus the drug loading capacity would be decreased compared with neat GO. However, even such a value of loading capacity is higher than that of the other common drug carrier materials such as polymer micelles and liposomes,[46–49] where the loading capacity is usually below 1 mg mg^{-1}.

We then incubated the aptamer-QD–GO–DOX nanocomposites with SK-N-SH cells at 0.5 mg mL^{-1} DOX concentration, which showed enhanced DOX delivery in comparison with SK-N-SH cells treated with free DOX, GO-DOX, and polyT$_{17}$–QD–GO–DOX (Fig. 7). The red fluorescence indicates the presence of DOX, while the green color arises from QDs. Fig. 7a–d indicate that the drug molecules rapidly accumulate inside the cells and are ultimately targeted to the cell nuclei after 3 h incubation, while the aptamer-QD–GO nanocomposites do not seem to cross the nuclear membrane and exist at the cell surface or in the cytoplasm. Previous studies have demonstrated that the release of DOX from the GO surface is pH-dependent,[11,12,45] and when the aptamer-QD–GO–DOX nanocomposites have been successfully internalized through specific aptamer-mediated endocytosis, the microenvironments in intracellular lysosomes and endosomes are acidic, which will afford active drug release from QD–GO delivery vehicles due to the increased hydrophilicity and solubility of DOX in acidic conditions, and then the released drug with recovered fluorescence can exclusively stain the nuclei as a result of the intercalation within the genomic DNA. Interestingly, only slight red emission of DOX is observed when incubating the SK-N-SH cells with GO–DOX or polyT$_{17}$–QD–GO–DOX under the same conditions (Fig. 7e–l), which is comparable to the control sample in the absence of any cellular transporters (Fig. 7m–p). The above results demonstrate that the GO with the extremely high aspect ratio could serve as a generic intracellular transporter with high drug loading efficiency, while the aptamer conjugated on the surface of the nanocomposites allows the targeted delivery of drug to the cells that express the aptamer target, and finally the unique fluorescence of the QDs facilitates imaging the internalization of the aptamer-QD–GO–DOX drug delivery system and tracing the transporting and the location of the carrier GO after the drug release, and in-depth research about this point is in progress. Notably, after being used as a drug delivery device *in vivo*, the GO might be cleared by tissues and/or biodegraded by enzymatic oxidation,[50] while the QDs used as cell imaging probes would be finally eliminated by organs.[51]

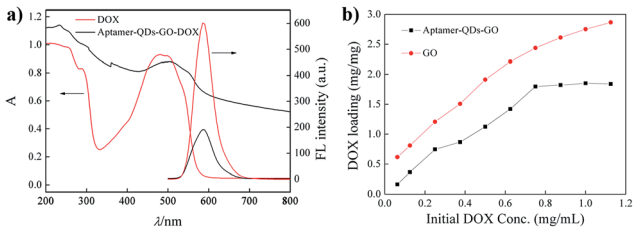

Fig. 6 (a) UV-vis and fluorescence spectra of DOX before and after adsorption on aptamer-QD–GO. (b) Loading capacity of DOX on aptamer-QD–GO nanocomposites and neat GO in different initial DOX concentrations.

Experimental

Preparation of GO

GO sheets were synthesized from natural graphite powder (Sinopharm Chemical Reagent Co., Ltd) by a modified Hummers method.[32,33] In detail, graphite powder (3 g), $K_2S_2O_8$ (2.5 g), and P_2O_5 (2.5 g) were added into a solution of concentrated H_2SO_4 (12 mL). The mixture was kept at 80 °C for 4.5 h. Subsequently, the mixture was cooled to room temperature and diluted with 0.5 L of Milli-Q purified water and left overnight. Then, the diluted mixture was filtered using a 0.45 μm microporous membrane and washed with water to remove the residual acid until the pH value of rinse water became neutral. The product was dried under room temperature overnight. This preoxidized graphite powder was then subjected to oxidation using Hummers' method. The preoxidized graphite powder was put into concentrated H_2SO_4 (120 mL) at 0 °C, $KMnO_4$ (15.0 g) was added gradually under stirring, and the temperature of the mixture was kept to be below 20 °C by ice-bath cooling, then the mixture was stirred at 35 °C for 2 h and then diluted with water (250 mL) in an ice bath to keep the temperature below 50 °C. The mixture was stirred for 2 h, and then an additional 0.7 L of water and 20 mL of 30% H_2O_2 were added. The mixture was filtered and washed with 1 : 10 HCl solution (1 L) in order to remove metal ions, and followed by 1 L of water to remove the acid until the water reached a neutral pH. The resulting solid was dried at 50 °C.

Published on 06 October 2014. Downloaded on 31/10/2014 00:31:00.

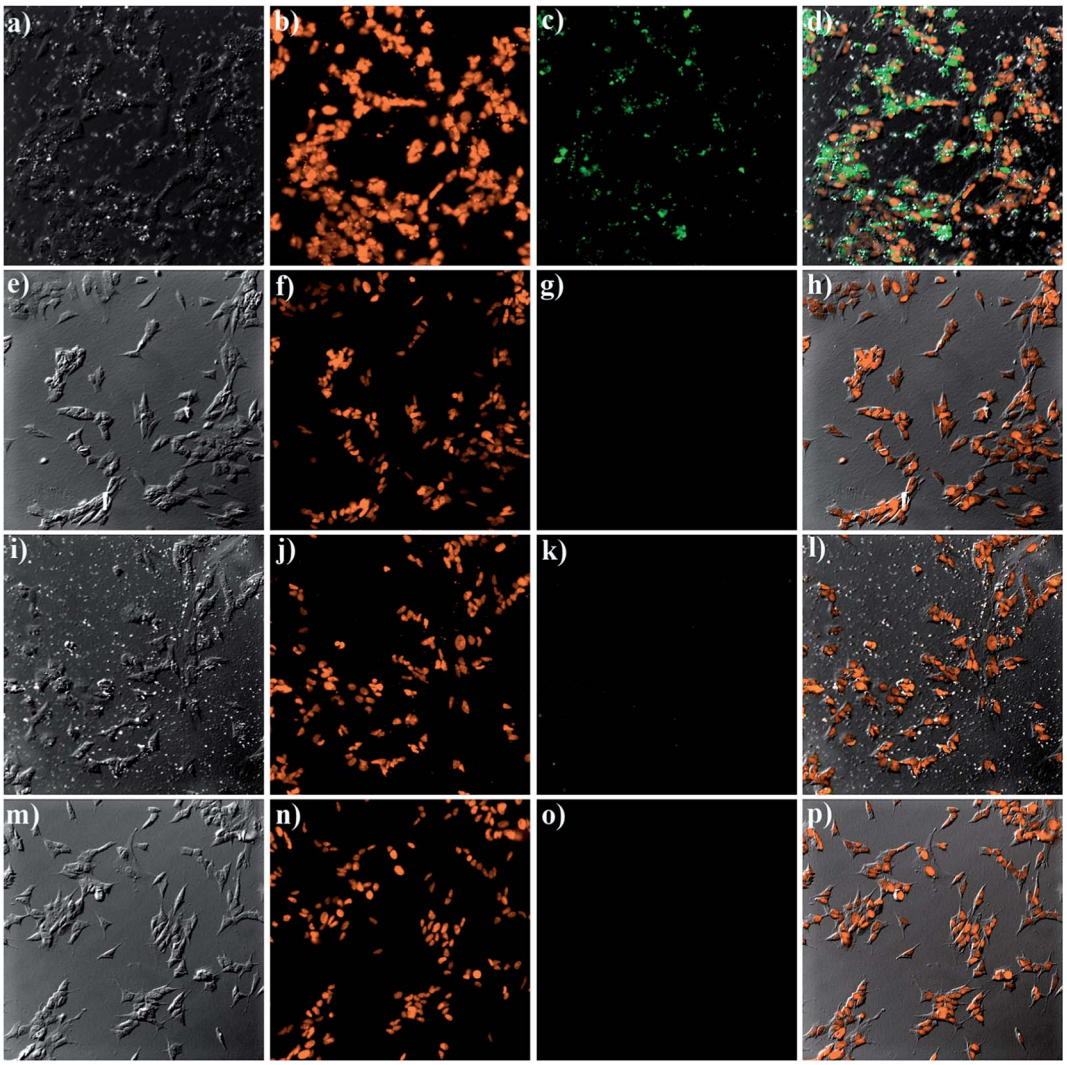

Fig. 7 Fluorescence images of SK-N-SH cells incubated for 3 h with (a)–(d) aptamer-QD–GO–DOX; (e)–(h) GO–DOX; (i)–(l) polyT_{17}–QD–GO–DOX; and (m)–(p) free DOX. (a, e, i, m) DIC images; (b, f, j, n) fluorescence images of DOX (red); (c, g, k, o) fluorescence images of QDs (green); (d, h, l, p) overlap of a corresponding fluorescence image and DIC image.

Surface modification of the QDs

Carboxyl modified CdSe@ZnS QDs (525 nm and 605 nm) were bought from Wu Han Jia Yuan Quantum Dots Co., Ltd. (Wuhan, China). 5 μL of 8 μM QDs, 8 μL of 100 μM amine-modified aptamer (the sequence was 5′-AAAAAAAAAACTTACGGTGGGG CAATT-3′), and 10 μL of 3 mg mL^{-1} 1-ethyl-3-(3-dimethyl-aminopropyl)carbodiimide (EDC) were added to 177 μL of 10 mM borate buffer (pH 7.4). After the mixture was kept shaking for 3.5 h (120 rpm, 25 °C), the aptamer modified QDs were purified using a membrane filter (MWCO, 30 kD) to remove excess aptamer, and the products were diluted with water for further use. A control aptamer without a poly A_{10} spacer was also modified on the surface of QDs with a similar process (the sequence was 5′-CTTACGGTGGGGCAATT-3′).

Fabrication of nanocomposites

A suitable amount of solid GO was added to the prepared aptamer-QD conjugates, the mixture was sonicated for 30 min, and then allowed to stand overnight so that undispersed GO sedimented. The resulting clear supernatant was carefully collected by centrifugation (16 000 rpm, 20 min) to remove the dissociative aptamer-QDs which undecorated on the GO sheets. The aptamer-QD–GO nanocomposites were resuspended with water and kept at 4 °C.

Characterization of the nanocomposites

UV-vis absorption spectra were recorded on a Shimadzu UV-2450 spectrophotometer (Tokyo, Japan). Steady-state fluorescence spectra were recorded on a Hitachi F-7000 fluorescence spectrofluorometer (Tokyo, Japan). The time-resolved fluorescence spectra were collected by using a FL-TCSPC fluorescence spectrophotometer (Horiba Jobin Yvon Inc., France). Transmission electron microscopy (TEM) measurements were conducted on a JEM-2010 transmission electron microscope (JEOL Ltd.). Atomic force microscopy (AFM) images were recorded with a Bruker MultiMode8 atomic force microscope.

 This journal is © The Royal Society of Chemistry 2014

Published on 06 October 2014. Downloaded on 31/10/2014 00:31:00.

AFM samples were prepared by drop casting the sample onto freshly cleaved mica surfaces, and dried under room temperature. Fluorescence imaging was performed with a DSU live-cell confocal microscope (Olympus, Japan) system, running the software Invivo 3.2/3D Analyzer 6.2 that was coupled to a Olympus IX81 microscope. Image analysis and processing were performed using Image-Pro® Plus Version 6.3 for Windows™.

Drug loading

DOX loading onto aptamer-QD–GO was done by simply mixing 0.5 mg mL^{-1} of DOX with the aptamer-QD–GO solution (~0.31 mg mL^{-1}) at pH 7.4 for 0.5 h and then stirred overnight at room temperature in the dark. Unbound excess DOX was removed by repeated centrifugation at 16 000 rpm for 10 min. The resulting aptamer-QD–GO–DOX complexes were re-suspended and stored at 4 °C. The amount of DOX loaded on aptamer-QD–GO was determined as follows. The DOX concentration in the upper layer was measured using a standard DOX concentration curve generated using the UV-vis spectrophotometer from a series of DOX solutions with different concentrations. The amount of DOX loaded on aptamer-QD–GO was determined using eqn (1)

$$\Phi = \frac{m_{DOX} - m'_{DOX}}{m_{GO}} \quad (1)$$

where Φ is the amount of DOX loaded on aptamer-QD–GO, m_{DOX} is the initial amount of DOX, m'_{DOX} is the amount of DOX in the upper layer, and m_{GO} is the amount of GO added.

Cell culture and imaging

SK-N-SH cells were cultured in flasks in minimum Eagle's essential medium (MEM) supplemented with 10% fetal bovine serum (FBS; Gibco) and 100 IU mL^{-1} penicillin–streptomycin at 37 °C under 5% humidified CO_2. Upon reaching confluence, the cells were trypsinized and replanted at a density of 1×10^6 cells per mL onto poly-L-lysine-coated coverslips and grown for 48 h. For the MTT assay, the medium was changed with 100 μL of fresh MEM (10% FBS) containing different amounts of aptamer-QD–GO, respectively, and the cells were allowed to grow for another 12 h (18 h, 24 h, 48 h). After adding 100 μL of MTT reagents at a concentration of 5 mg mL^{-1} into each well, the cells were allowed to grow for another 4 h. The medium was then removed and 100 μL of DMSO was added. Finally, the absorption at 490 nm was measured with a Molecular Devices Spectra-Max 190 Microplate Reader (California, USA). For cellular uptake studies, the cells were rinsed gently with prewarmed phosphate-buffered saline (PBS) and incubated with aptamer-QD–GO–DOX (free DOX, GO–DOX, or polyT_{17}–QD–GO–DOX) at an initial DOX concentration of 0.5 mg mL^{-1} in MEM for 3 h at 37 °C. After that, the cells were gently rinsed twice with PBS, and then fixed and mounted for microscopy observation.

Conclusions

In this study, a novel, multifunctional aptamer-QD–GO nanocomposite has been developed through the linkage of DNA aptamer to serve as an imaging agent and a drug delivery scaffold. These results were made possible by the use of a suitable nanosized spacer (poly A_{10}) that separated the QDs and the GO, thereby reducing fluorescence quenching. Meanwhile, the extremely high aspect ratio of GO as well as the specific recognization between the aptamer and the membrane protein make the nanocomposite a good scaffold capable of cell-targeted drug delivery with an enhanced activity compared to monovalent drugs, the QDs also served as an optical indicator for the endocytic and the drug delivery process. Such nanoplatforms with built-in capabilities for *in situ* imaging, treatment and monitoring are expected to open a new avenue for therapy in general, possibly leading to clinical applications.

Acknowledgements

This work was supported by the National Natural Science Foundation of China (Grant no. 1035005, 21105044 and 21205011).

Notes and references

1 K. P. Loh, Q. Bao, G. Eda and M. Chhowalla, *Nat. Chem.*, 2010, **2**, 1015–1024.
2 K. S. Novoselov, Z. Jiang, Y. Zhang, S. V. Morozov, H. L. Stormer, U. Zeitler, J. C. Maan, G. S. Boebinger, P. Kim and A. K. Geim, *Science*, 2007, **315**, 1379.
3 C. N. R. Rao, A. K. Sood, R. Voggu and K. S. Subrahmanyam, *J. Phys. Chem. Lett.*, 2010, **1**, 572–580.
4 D. A. Dikin, S. Stankovich, E. J. Zimney, R. D. Piner, G. H. B. Dommett, G. Evmenenko, S. T. Nguyen and R. S. Ruoff, *Nature*, 2007, **448**, 457–460.
5 F. Bonaccorso, Z. Sun, T. Hasan and A. C. Ferrari, *Nat. Photonics*, 2010, **4**, 611–622.
6 J. H. Jung, D. S. Cheon, F. Liu, K. B. Lee and T. S. Seo, *Angew. Chem., Int. Ed.*, 2010, **49**, 5708–5711.
7 S.-H. Hu, Y.-W. Chen, W.-T. Hung, I. W. Chen and S.-Y. Chen, *Adv. Mater.*, 2012, **24**, 1748–1754.
8 P. V. Kamat, *J. Phys. Chem. Lett.*, 2010, **1**, 520–527.
9 Z. Liu, J. T. Robinson, X. Sun and H. Dai, *J. Am. Chem. Soc.*, 2008, **130**, 10876–10877.
10 V. K. Rana, M.-C. Choi, J.-Y. Kong, G. Y. Kim, M. J. Kim, S.-H. Kim, S. Mishra, R. P. Singh and C.-S. Ha, *Macromol. Mater. Eng.*, 2011, **296**, 131–140.
11 L. Zhang, J. Xia, Q. Zhao, L. Liu and Z. Zhang, *Small*, 2010, **6**, 537–544.
12 X. Sun, Z. Liu, K. Welsher, J. T. Robinson, A. Goodwin, S. Zaric and H. Dai, *Nano Res.*, 2008, **1**, 203–212.
13 L. Zhang, S. J. Zhen, Y. Sang, J. Y. Li, Y. Wang, L. Zhan, L. Peng, J. Wang, Y. F. Li and C. Z. Huang, *Chem. Commun.*, 2010, **46**, 4303–4305.
14 Y. Wang, S. J. Zhen, Y. Zhang, Y. F. Li and C. Z. Huang, *J. Phys. Chem. C*, 2011, **115**, 12815–12821.
15 Y. Xu, Z. Liu, X. Zhang, Y. Wang, J. Tian, Y. Huang, Y. Ma, X. Zhang and Y. Chen, *Adv. Mater.*, 2009, **21**, 1275–1279.
16 A. Midya, V. Mamidala, J.-X. Yang, P. K. L. Ang, Z.-K. Chen, W. Ji and K. P. Loh, *Small*, 2010, **6**, 2292–2300.

Published on 06 October 2014. Downloaded on 31/10/2014 00:31:00.

17 I. L. Medintz, H. T. Uyeda, E. R. Goldman and H. Mattoussi, *Nat. Mater.*, 2005, **4**, 435–446.
18 C. Zhang, J. Xu, S. Zhang, X. Ji and Z. He, *Chem.–Eur. J.*, 2012, **18**, 8296–8300.
19 L. Chen, X. Zhang, G. Zhou, X. Xiang, X. Ji, Z. Zheng, Z. He and H. Wang, *Anal. Chem.*, 2012, **84**, 3200–3207.
20 M. Liu, H. Zhao, X. Quan, S. Chen and X. Fan, *Chem. Commun.*, 2010, **46**, 7909–7911.
21 L. Q. Chen, S. J. Xiao, P. P. Hu, L. Peng, J. Ma, L. F. Luo, Y. F. Li and C. Z. Huang, *Anal. Chem.*, 2012, **84**, 3099–3110.
22 A. Cao, Z. Liu, S. Chu, M. Wu, Z. Ye, Z. Cai, Y. Chang, S. Wang, Q. Gong and Y. Liu, *Adv. Mater.*, 2010, **22**, 103–106.
23 X.-Y. Yu, Z.-H. Chen, D.-B. Kuang and C.-Y. Su, *ChemPhysChem*, 2012, **13**, 2654–2658.
24 G. Katsukis, J. Malig, C. Schulz-Drost, S. Leubner, N. Jux and D. M. Guldi, *ACS Nano*, 2012, **6**, 1915–1924.
25 L.-L. Li, K.-P. Liu, G.-H. Yang, C.-M. Wang, J.-R. Zhang and J.-J. Zhu, *Adv. Funct. Mater.*, 2011, **21**, 869–878.
26 H. Dong, W. Gao, F. Yan, H. Ji and H. Ju, *Anal. Chem.*, 2010, **82**, 5511–5517.
27 P. Tuan Anh, C. Byung Choon and J. Yeon Tae, *Nanotechnology*, 2010, **21**, 465603.
28 Y. Wang, H.-B. Yao, X.-H. Wang and S.-H. Yu, *J. Mater. Chem.*, 2011, **21**, 562–566.
29 M.-L. Chen, J.-W. Liu, B. Hu, M.-L. Chen and J.-H. Wang, *Analyst*, 2011, **136**, 4277–4283.
30 M. Grzelczak, M. A. Correa-Duarte, V. Salgueiriño-Maceira, M. Giersig, R. Diaz and L. M. Liz-Marzán, *Adv. Mater.*, 2006, **18**, 415–420.
31 K. Takemura, P. Wang, I. Vorberg, W. Surewicz, S. A. Priola, A. Kanthasamy, R. Pottathil, S. G. Chen and S. Sreevatsan, *Exp. Biol. Med.*, 2006, **231**, 204–214.
32 W. S. Hummers and R. E. Offeman, *J. Am. Chem. Soc.*, 1958, **80**, 1339.
33 Y. Xu, H. Bai, G. Lu, C. Li and G. Shi, *J. Am. Chem. Soc.*, 2008, **130**, 5856–5857.
34 Z. Zhang, Y. Shi, Y. Pan, X. Cheng, L. Zhang, J. Chen, M.-J. Li and C. Yi, *J. Mater. Chem. B*, 2014, **2**, 5020–5027.
35 C. Le-Tien, R. Lafortune, F. Shareck and M. Lacroix, *Talanta*, 2007, **71**, 1969–1975.
36 C.-H. Lu, H.-H. Yang, C.-L. Zhu, X. Chen and G.-N. Chen, *Angew. Chem., Int. Ed.*, 2009, **48**, 4785–4787.
37 S. He, B. Song, D. Li, C. Zhu, W. Qi, Y. Wen, L. Wang, S. Song, H. Fang and C. Fan, *Adv. Funct. Mater.*, 2010, **20**, 453–459.
38 Z. Luo, Y. Lu, L. A. Somers and A. T. C. Johnson, *J. Am. Chem. Soc.*, 2009, **131**, 898–899.
39 S. Kaniyankandy, S. Rawalekar and H. N. Ghosh, *J. Phys. Chem. C*, 2012, **116**, 16271–16275.
40 Z. Lu, C. X. Guo, H. B. Yang, Y. Qiao, J. Guo and C. M. Li, *J. Colloid Interface Sci.*, 2011, **353**, 588–592.
41 B. Pan, D. Cui, C. S. Ozkan, M. Ozkan, P. Xu, T. Huang, F. Liu, H. Chen, Q. Li, R. He and F. Gao, *J. Phys. Chem. C*, 2008, **112**, 939–944.
42 M. Zheng, A. Jagota, E. D. Semke, B. A. Diner, R. S. McLean, S. R. Lustig, R. E. Richardson and N. G. Tassi, *Nat. Mater.*, 2003, **2**, 338–342.
43 M. Zheng, A. Jagota, M. S. Strano, A. P. Santos, P. Barone, S. G. Chou, B. A. Diner, M. S. Dresselhaus, R. S. Mclean, G. B. Onoa, G. G. Samsonidze, E. D. Semke, M. Usrey and D. J. Walls, *Science*, 2003, **302**, 1545–1548.
44 W. R. Algar, D. Wegner, A. L. Huston, J. B. Blanco-Canosa, M. H. Stewart, A. Armstrong, P. E. Dawson, N. Hildebrandt and I. L. Medintz, *J. Am. Chem. Soc.*, 2012, **134**, 1876–1891.
45 X. Yang, X. Zhang, Z. Liu, Y. Ma, Y. Huang and Y. Chen, *J. Phys. Chem. C*, 2008, **112**, 17554–17558.
46 F. Li, M. Danquah and R. I. Mahato, *Biomacromolecules*, 2010, **11**, 2610–2620.
47 M. P. Baranello, L. Bauer and D. S. W. Benoit, *Biomacromolecules*, 2014, **15**, 2629–2641.
48 W. Sun, N. Zhang, A. Li, W. Zou and W. Xu, *Int. J. Pharm.*, 2008, **353**, 243–250.
49 K.-J. Chen, E.-Y. Chaung, S.-P. Wey, K.-J. Lin, F. Cheng, C.-C. Lin, H.-L. Liu, H.-W. Tseng, C.-P. Liu, M.-C. Wei, C.-M. Liu and H.-W. Sung, *ACS Nano*, 2014, **8**, 5105–5115.
50 C. Bussy, H. Ali-Boucetta and K. Kostarelos, *Acc. Chem. Res.*, 2013, **46**, 692–701.
51 M. Longmire, P. L. Choyke and H. Kobayashi, *Nanomedicine*, 2008, **3**, 703–717.

 This journal is © The Royal Society of Chemistry 2014